REPORT DOCUMENTATION PAGE

Form Approved OMB NO. 0704-0188

1. REPORT DATE (DD-MM-YYYY)	2. REPORT TYPE	3. DATES COVERED (From - To)
12-05-2023	Final Report	1-May-2022 - 30-Apr-2023

4. TITLE AND SUBTITLE
Final Report: Twisted graphene-based Josephson junction detectors

5a. CONTRACT NUMBER

5b. GRANT NUMBER
W911NF-22-P-0026

5c. PROGRAM ELEMENT NUMBER

6. AUTHORS

5d. PROJECT NUMBER

5e. TASK NUMBER

5f. WORK UNIT NUMBER

7. PERFORMING ORGANIZATION NAMES AND ADDRESSES
Truventic LLC
737 Maryland AV

Winter Park, FL 32789 -0000

8. PERFORMING ORGANIZATION REPORT NUMBER

9. SPONSORING/MONITORING AGENCY NAME(S) AND ADDRESS (ES)
U.S. Army Research Office
P.O. Box 12211
Research Triangle Park, NC 27709-2211

10. SPONSOR/MONITOR'S ACRONYM(S)
ARO

11. SPONSOR/MONITOR'S REPORT NUMBER(S)
80437-OD-ST1.3

12. DISTRIBUTION AVAILIBILITY STATEMENT
2 Approved for public release; distribution is unlimited

13. SUPPLEMENTARY NOTES
The views, opinions and/or findings contained in this report are those of the author(s) and should not contrued as an official Department of the Army position, policy or decision, unless so designated by other documentation.

14. ABSTRACT

15. SUBJECT TERMS

16. SECURITY CLASSIFICATION OF:			17. LIMITATION OF ABSTRACT	15. NUMBER OF PAGES	19a. NAME OF RESPONSIBLE PERSON
a. REPORT	b. ABSTRACT	c. THIS PAGE			Coleman Cariker
UU	UU	UU	UU		19b. TELEPHONE NUMBER 321-230-8855

RPPR

as of 03-Jul-2023

Agency Code:

Proposal Number: **Agreement Number:**

Organization:
Address: , ,
Country:
DUNS Number: EIN:
Report Date: Date Received:
for Period Beginning and Ending
Title:
Begin Performance Period: **End Performance Period:**
Report Term: -
Submitted By: Email:
Phone:

Distribution Statement: -

STEM Degrees: **STEM Participants:**

Major Goals:

Accomplishments:

Training Opportunities:

Results Dissemination:

Plans Next Period:

Honors and Awards:

Protocol Activity Status:

Technology Transfer:

I certify that the information in the report is complete and accurate:
Signature:
Signature Date:

Antenna-Coupled Graphene Josephson-Junction Terahertz and Millimeter Wave Detector

Report authors: Robert E. Peale,[1,2] F. Javier Gonzalez,[1] Michael S. Lodge,[2] Masahiro Ishigami,[2,3] Richard A. Klemm,[2] Ami Rathod,[2] Kirsten L. Lina,[2] Anna C. Bowman,[2] Francisco Hernandez,[2] Chris J. Fredricksen,[1] Coleman Cariker[1]

Affiliations: [1]Truventic LLC, 1209 W. Gore St. Orlando FL 32816, [2]Physics Department, University of Central Florida, Orlando FL 32816, [3]Nanoscience Center, University of Central Florida, Orlando FL 32816.

Abstract

Highly-sensitive broadly-tunable detectors are needed for future multi-domain sensing and quantum-information systems. Layered graphene with "magic" twist-angle between 2 - 4 sheets is superconducting below ~2 K. Demonstrated Josephson junctions in this material feature very high dynamic resistance at the maximum zero-voltage current. Biased at this current, a small microwave voltage across the junction shifts the voltage-current step, which results in a large DC output voltage. A suitable antenna driven by external radiation can source the enabling AC voltage across the junction. Detection by this non-thermal mechanism may be both fast and sensitive. Our calculations indicate a noise-equivalent detectable photon flux of 1 photon per 6 ns. Additionally, there is a bolometric response, whose temperature coefficient of resistance we estimate to have the promisingly high value 300%/K. Design, fabrication, response, twist-angle tolerance, and characterization for antenna-coupled, superconducting-graphene, Josephson-junction detectors of mm-wave and THz radiation are reported.

Introduction and background

Several reports of graphene-based Josephson junction (JJ) bolometers demonstrate astonishing sensitivity at the single-photon level for microwave-to-visible wavelengths [1-5]. These JJs have used graphene as the normal weak link between two conventional superconductors. Their bolometric sensitivity is due in part to slow thermalization of heated electrons to the lattice temperature, and their speed is due to the small heat capacity of graphene.

Additionally, there has been a report of bolometric response in superconducting magic-angle twisted bilayer graphene at 1.55 μm wavelength (with no JJ) [6]. A remarkably high temperature coefficient of resistance of 300%/K was demonstrated.

Josephson junctions fabricated entirely out of superconducting magic-angle twisted multilayer graphene have been reported [7]. In any JJ detectors, there is a "video" mechanism [8] in addition to a bolometric mechanism. The former does not require the absorption of thermal energy at the JJ weak link, in contrast to the bolometer. The video mechanism requires only the appearance of an AC voltage across the JJ, without heat, so it is not limited by thermal considerations. We have published our estimate for sensitivity of the video mechanism in antenna-coupled all-graphene JJ detectors [9], where we suggested a noise equivalent detectable photon flux of 1 per 6 ns at sub-millimeter wavelengths. That analysis is repeated in this report.

A feature of the non-thermal video mechanism is that it has "very great speed advantage over the bolometer" [8]. This makes the video mechanism uniquely attractive for certain single-photon applications. A hyper-sensitive bolometer might be preferred for applications such

as detection of dark matter axions [10,11], which do not require high speed. A faster detector would be preferred for applications such as quantum communication for high single-photon bit rates [12,13]. Any parasitic slow bolometric response might be quenched by thermal anchoring without affecting the video response at all.

Magic-angle graphene (MAG) is only superconducting when properly gated to adjust the Fermi level into the region of the band structure flattened by the twist. The weak link is also created by gating [7]. This sensitivity to gating allows one to turn the detector off when signal is not expected, and gated detection is a well-established method for reducing detector noise. Gating might also be used creatively to enable additional functionality, for instance to select between differently oriented antennas for polarization selection. Such selection is needed in the BB84 protocol for quantum cryptography [12].

Figure 1 presents schematics for our device design. The magic-angle graphene (MAG) is sandwiched between hexagonal boron nitride gate dielectrics. The Fermi-level is manipulated by a voltage applied to a uniform bottom gate, so that superconductivity will appear when the level is at the flat-band created by the twist between graphene sheets. Top gates provide additional control, so that the superconductivity can be confined to regions on either side of a normal weak link, thus creating the JJ. On either end, the graphene is contacted by the tips of a bowtie antenna, which collects the external radiation and sources AC current to the JJ. DC current bias is applied, and DC voltage response measured, via the source (S) and drain (D) antenna contacts.

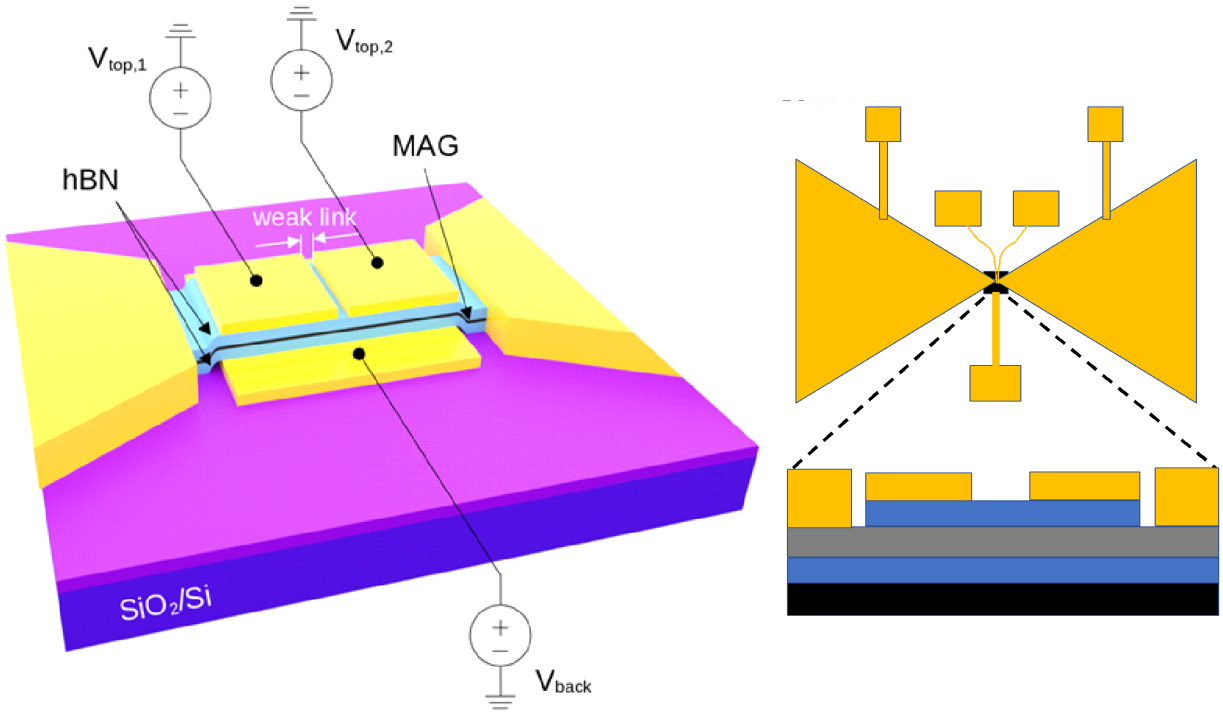

Figure 1. Schematics of antenna-coupled superconducting magic angle graphene Josephson junction detector. Relative dimensions are not to scale. S = source, D = drain, TG = top gate, BG = back gate, hBN = hexagonal boron nitride, MAG = magic-angle graphene.

Antennas collect THz/mm-wave radiation with an effective area that is orders of magnitude larger than any possible graphene sensing element alone. Absorption is 100% for radiation that falls within an antenna's effective area by definition [14], while the direct photon absorption of graphene itself is thought to be less than 10% [6]. The excited antenna currents are concentrated in the JJ load, thus amplifying the AC voltage across the JJ that is responsible for the video detection mechanism. Antennas also provide wavelength and polarization selectivity [15]. They are easily fabricated into arrays and may be combined in series or parallel to enhance DC output voltage or current, respectively. The antenna function is largely independent of temperature, and it is accurately predicted by numerical electrodynamic simulations. Antenna coupling separates collection and detection functions, so that each can be independently optimized [14].

Results

The Phase I results section is organized by proposal objective. Accomplishments are given under each objective.

Base Objectives 1 & 2, and Option Objective 3: Predictive model, detector design, design iteration.

Base Objective 1 was to develop a predictive model. Base Objective 2 was to develop a detector design. Option Objective 3 was to iterate the design. Activities and results of these three objectives were mutually informative and inseparable, so they are presented together.

Figure 2 (left) compares COMSOL simulations of open-circuit voltage at the antenna feed for four different antenna designs [14]. A THz resonance is observed. The bowtie gives the highest AC voltage, informing the selection of the bowtie for our detector design. Figure 2 (right) presents the current through an 800 Ω load at the feed of a bowtie antenna for 1 pW/μm^2 incident intensity. The inset shows the calculated AC current distribution in the antenna and its concentration at the feed.

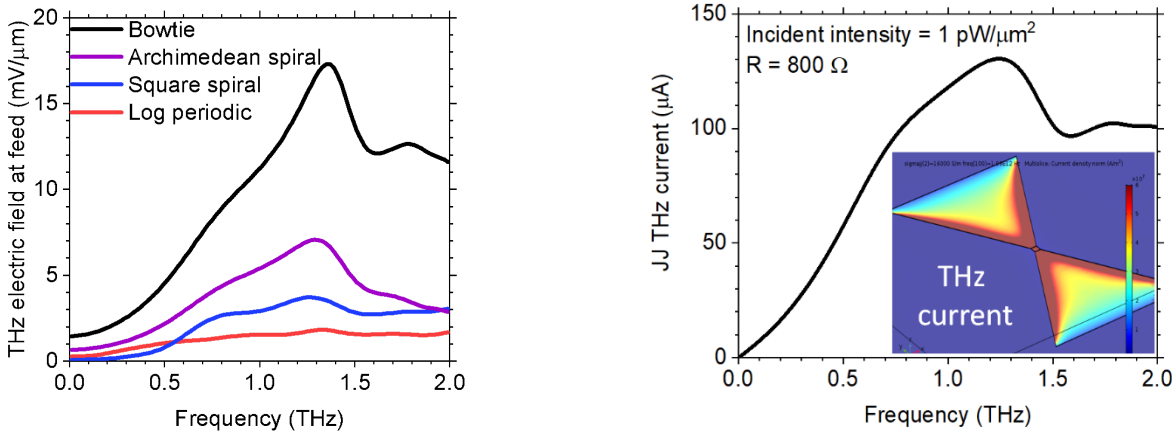

Figure 2. (Left) COMSOL simulations of electric field at the feed for various antenna designs with no load. (Right) COMSOL simulation of current for bowtie antenna with 800 Ω load and 1 pW/μm^2 incident intensity. (inset) Current distribution in the bowtie, which has 80 μm length.

Figure 3 (left) presents JJ Voltage-Current (VI) curves replotted from [7]. In the video detector mechanism, the maximum zero voltage current I_1 (JJ switching current) is depressed when an AC voltage appears across the JJ. Such a voltage appears when an AC current is driven through a JJ load, sourced by an antenna, because the AC impedance of the JJ is non-zero even when the DC resistance is zero. The device is current biased at the dark value of I_1. When mm-waves or THz are absorbed by a suitable antenna with the JJ at its feed, I_1 shifts below the bias current, and a DC voltage appears across the JJ. The sensitivity of the video detection mechanism depends on the dynamic resistance (steepness) of the VI curve at the bias point.

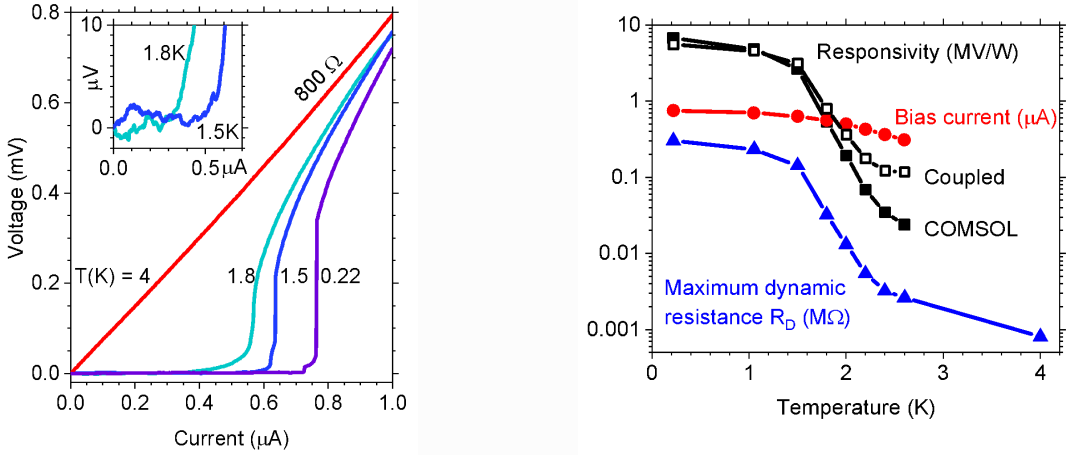

Figure 3. (left) Voltage-current curves for superconducting-graphene Josephson junction from ref. [7]. JJ temperatures are indicated next to each curve. The inset is a blow-up to reveal the ~1 μV noise level. (right) Temperature dependence of optimum DC current bias, dynamic resistance at the bias point, and responsivity calculated by numerical (COMSOL) and analytical (Coupled) methods,

The resistively shunted junction (RSJ) model for JJ detectors comprises an ideal junction with only pair tunnelling current and a parallel shunt resistor R that carries only quasiparticle current. The value of R is the normal state resistance [3], which according to Fig. 3 (left) is 800 Ω. THz photon energies exceed the superconducting gap, so THz currents pass mainly through R. Additional inductive reactance determined from the Josephson equations [8] depends on AC current, so its estimation is complicated. We assume R, the lower bound on impedance, for our responsivity estimates.

The shift in the maximum zero-voltage current of a Josephson junction is [8]

$$\delta I_1 = -\left(\frac{2eV_{THz}}{\hbar\omega}\right)^2 \frac{I_1}{4} \quad . \tag{1}$$

The squared factor is the ratio of the pair energy difference across the junction to the photon energy. We assume the detector is DC current biased at I_1, which we take to be the point with the maximum dynamic resistance

$$R_D = dV/dI. \tag{2}$$

R_D and I_1 are found from the DC transport curves Fig. 3 (left) and are plotted as function of temperature in Fig. 3 (right). The shift results in a DC output voltage

$$\delta V_{out} = R_D \delta I_1, \tag{4}$$

and this response is proportional to absorbed power. With impedance mismatch between antenna and load already accounted for in the COMSOL simulation, the maximum I_{THz} = 130 μA (Fig. 2, right) gives an absorbed power $I_{THz}^2 R$ = 13.5 μW at 1.25 THz. The temperature dependence of the responsivitiy (δV_{out} / absorbed power) is plotted as solid black symbols in Figure 3 (right) and labeled "COMSOL". The maximum value is 7 MV/W. Responsivity is ~10x smaller at T = 1.7 K than at 0.3 K.

Alternatively, the *coupled* power responsivity for a JJ detector is

$$S = R_D/2I_1 R\Omega^2, \tag{5}$$

where $\pi\Omega$ is approximately the ratio of photon energy to gap [8]. At 1.25 THz, $\Omega \sim 5$. The impedance of the bowtie acting as a current source is 300 Ω at the 1.25 THz resonance, so that it will couple 55% of the absorbed optical power to an 800 Ω load at its feed. Accounting for this mismatch, we obtain the responsivity curve given by open square symbols in Figure 3 (right) and labeled "coupled". The results agree well with those of the COMSOL simulation over most of the temperature range. Since the impedance of a bowtie can be adjusted by changing its shape, responsivity can be improved.

By expanding the V-I data from [7], we find the broad-spectrum noise amplitude to be ~1 μV, as shown in the inset of Figure 3 (left). Thus, the noise equivalent power (NEP) is not worse than 0.14 pW. It would be much smaller (better) if we restricted the noise spectral bandwidth to just 1 Hz, as is usually done via lock-in detection. An NEP of 0.14 pW, corresponds to a photon flux at 1.25 THz of ~1 photon every 6 ns. The prospects for single photon detection seem good.

The I_1 value also shifts down and the VI curve becomes less steep with increasing temperature, Fig. 4 (left), giving rise to a bolometric detection mechanism. For such thermal detectors, speed is determined by the thermal time-constant, which is short for graphene due to its small heat capacity. However, the non-bolometric "video" mechanism is thought to be faster and still very sensitive [8]. Experimentally, excellent thermal grounding could suppress a bolometric contribution to a video detector. However, for some single-photon applications, such as quantum LIDAR [16] and Dark Matter Axion detection [10,11], speed may not be as critical. Then, a bolometric mechanism might be preferred, and the antenna could be configured to source heat as opposed to an AC current to the JJ. This can be achieved by making the antenna arms orthogonal to the JJ current direction.

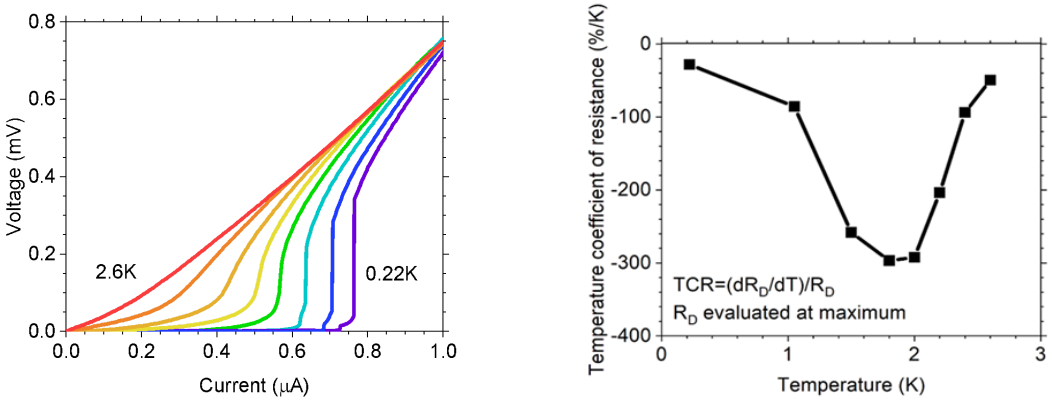

Figure 4. Voltage-current curves for 4-layer magic angle twist graphene Josephson junction [7]. Temperatures are 0.22, 1.05, 1.5, 1.8, 2.0, 2.2, 2.4, and 2.6 K, with the end values indicated. (right) Temperature coefficient of resistance vs temperature.

Figure 3 (right) presented a plot of R_D versus T. From these data we obtain the temperature coefficient of resistance (TCR), which is plotted in Figure 4 (right). Bolometer responsivity is proportional to TCR. The maximum occurs at 1.9 K and has the value -300%/K. This value is ~100x better than for room temperature VO_x [17], the standard material for long-wave IR bolometers. The temperature 1.9 K is easily obtained in a pumped-liquid-helium optical cryostat.

Proper twist angle is needed for graphene superconductivity. Deviation from the magic twist angle decreases T_c. From empirical T_c vs. n/n_s data [7], where n is the gate-controlled electron concentration, and the twist-dependent band density of states n_s is known as function of twist angle, we created a plot of T_c vs twist angle, Figure 5 (left). Reducing T_c at fixed T should effect responsivity similarly as raising T at fixed T_c. Thus, from Figure 5 (left) and Figure 3 (right), we obtain R_D vs twist angle. Responsivity of video JJ detectors is proportional to R_D, Eq. (5). Using maximum responsivity predicted for the video mechanism, we obtain the curve plotted in Figure 5 (right). The full width at half maximum is about 0.1 deg, so that twist angle accuracy should be better than this. Our electrically-controlled stacking-station turn-table has 0.004 deg accuracy.

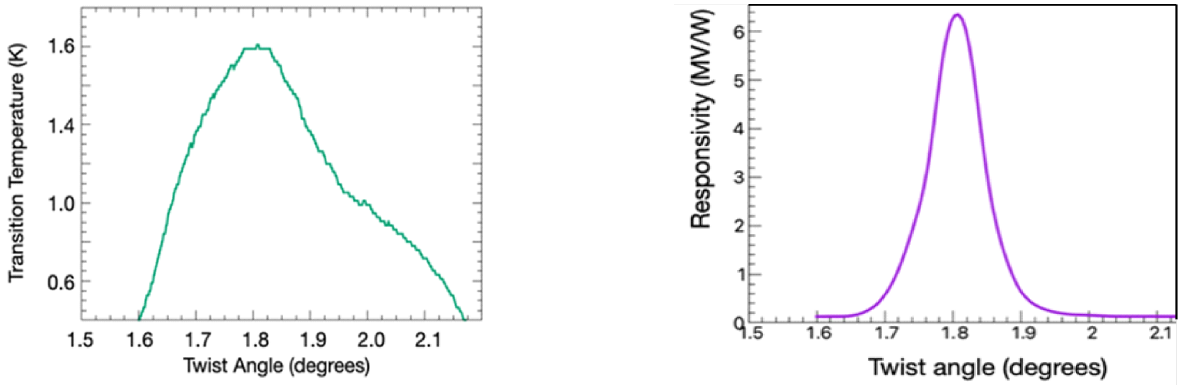

Figure 5. (left) T_c as a function of twist angle. (right) Responsivity vs twist angle.

<u>Base Objective 3 and Option Objective 2. Develop fabrication plan and characterize fabricated components.</u>

These objectives are mutually informative, and hence will be summarized together. Device fabrication first builds a magic angle graphene stack, fully encapsulated with hexagonal boron nitride (hBN) flakes, using a cut-and-stack method described in [6]. Single layer graphene is exfoliated on a wafer with electron-beam patterned location markers and confirmed by micro-Raman spectroscopy. Exfoliated hBN flakes are produced similarly. We use pyramidal polydimethylsiloxane (PDMS) stamps having ~180 μm plateau edge length to handle exfoliated flakes via a sacrificial poly(bisphenol A carbonate) (PC) film as an interface layer between hBN and the PDMS [18]. The 20-80 nm thick hBN encapsulating flakes serve as gate dielectrics. Figure 6 (left) presents a photograph of the custom stacking apparatus that we assembled for this process.

A back gate was prefabricated via electron beam lithography with 2.5 nm Cr and 40 nm Au. Then, a flake of 20-80 nm thick hBN (2D Semiconductors) was transferred onto the back gate and annealed at 500°C under flowing ultra-high purity O_2 and Ar gases to remove residues from the transfer process [19]. Next, a stack of 20-80 nm hBN and twisted bilayer graphene (NGS Naturgraphit), having a twist angle of about 1.1°, was built on another pyramidal trunk stamp having a PC (Sigma 181625) interface layer [18]. The surfaces of graphene-on-stamp and hBN-on-back gate were then inspected via atomic force microscopy (AFM) to identify clean, bubble-free regions. The hBN-twisted graphene stack was aligned and released onto the hBN on back gate such that the cleanest parts of each surface interface together. Each flake was picked up at a temperature of 110°C and released from the stamp at 175°C. Fabrication has been completed up to this step. Figure 6 (right) presents an optical microscope image with the flake edges indicated by dashed lines.

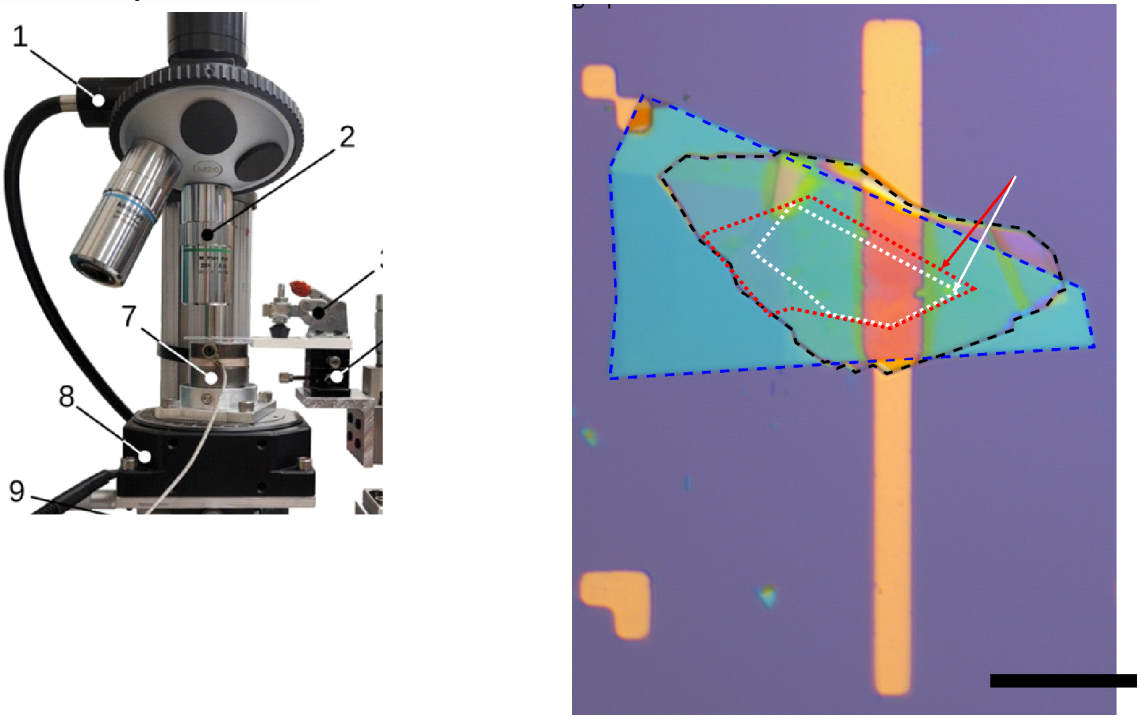

Figure 6. (left) Photograph of stacking station comprising an optical microscope with (1) a fiber-guided, in-line white illumination source and (2) long focal-length, plan apochromat, infinity-corrected objectives; the stamp manipulator with (3) a toggle clamp, (4) a tilt-tip goniometer, (5) 3-axis translation stage, and (6) a long-throw, motorized translation stage; and the wafer manipulator with (7) a heated vacuum chuck, (8) a

motorized rotation stage, and (9) a 2-axis translation stage. (right) Microscope image of hBn/graphene/twist-graphene/hBn on back gate.

Edge contacts will be made to the graphene using standard electron beam lithography and plasma etching techniques [20]. A top gate structure having a narrow channel to define the weak link region in the graphene will then be lithographically defined, after which the antenna, interconnects, and bond pads will be similarly defined and metalized. Next, we will apply bottom-gate contacts and top gates by electron-beam lithography for bias control of the Fermi level and creation of the JJ weak link, respectively.

Bowtie antennas will be fabricated by contact photolithography with the stack placed at the feed of the antenna. For training purposes in photolithography and mm-wave characterization, and to verify the predicted resonance response, Au bowtie antennas with Au/Sb_2Te_3 thermocouple junctions at their feed have been fabricated, as shown in Figure 7.

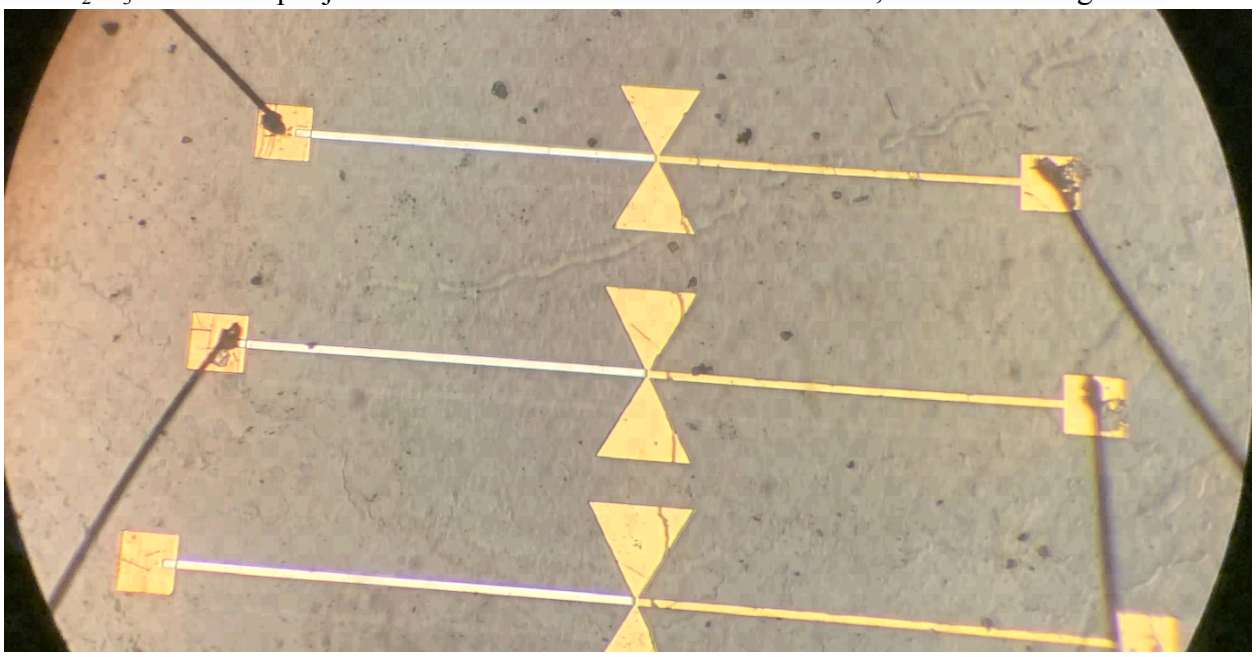

Figure 7. Microscope image of antenna coupled Au/Sb_2Te_3 thermocouple detectors on SiO_2 wafer. Bowtie antennas of ~0.4 mm length are designed for 200 GHz resonance.

Base objective 4 and Option objective 2: Characterization plan and device characterization

We will first measure the DC and rf electronic properties of the magic angle graphene and JJ in a 40 mK cryostat operated as a fee-based user facility by U Mass Boston, Prof. Matt Bell. Figure 8 (left) presents a photograph of this cryostat. Figure 8 (right) shows a mock-up of part of an enclosure for the sample. Pin feedthroughs are for DC sourcing and measurement via twisted pairs. The SMA feedthrough is for testing of photo response to 10 GHz AC voltage. The box must be designed to enable wire bonding after the chip carrier is mounted in the box and wired to the feed throughs to avoid blowing the device. After wire bonding, any manipulations that might electrically disturb the device must be avoided. The devices must be grounding while making any electrical connections. The finalized box design will be fabricated from oxygen free copper. For THz characterization in the 40 mK cryostat, which lacks external optical access, we plan to use a thermal source with THz bandpass filter filtering [21].

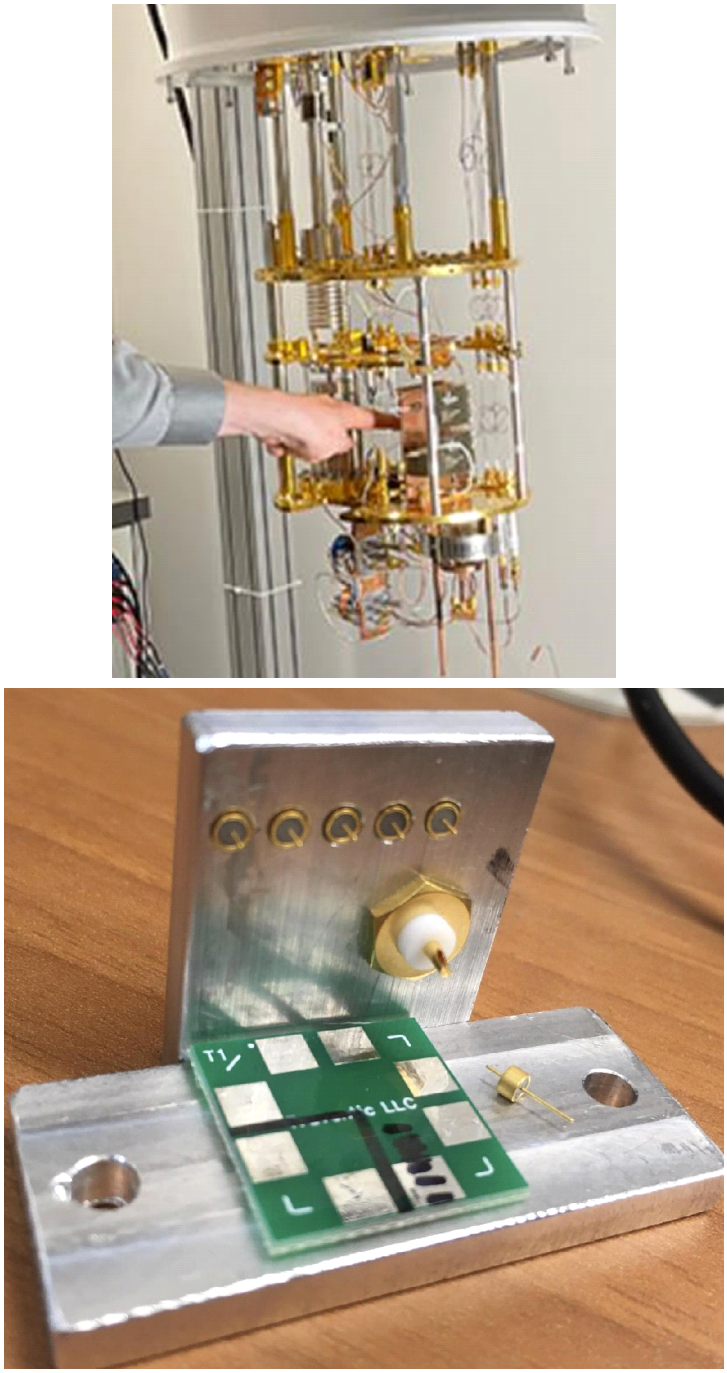

Figure 8 (left). U Mass Boston dry dilution refrigerator. (right) Aluminum mock-up of Copper sample box for mounting in UMB cryostat.

Optical measurements will be performed at UCF using a Janis 8DT cryostat with immersion in pumped superfluid He at 1.7 K. The source will be a backward wave oscillator (BWO, Microtech Instruments) tunable from 160 GHz to 1.4 THz. A photograph of the BWO, which was an equipment donation from the U.S. Air Force Research Lab WPAFB, is presented in Figure 9 (left). Figure 9 (right) shows that we are successfully used this source to characterize other types of antenna-coupled THz detectors [22].

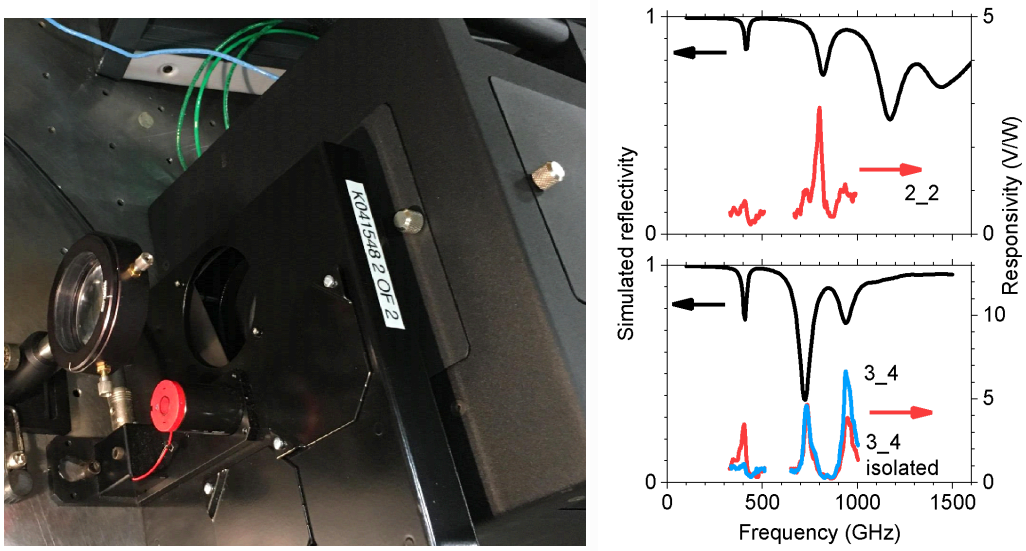

Figure 9 (left) Photograph of BWO head, chopper, and TPX lens. (right) Demonstration of antenna-coupled detector characterization using our BWO, together with electrodynamic simulations [22].

Summary

This Phase I STTR effort established the design for an antenna-coupled Josephson junction detector entirely fabricated from superconducting graphene with promise for single-photon detection at terahertz and millimeter wavelengths. It predicted the responsivity and a promising noise equivalent detectable photon flux for the video detection mechanism. It predicted a large temperature coefficient of resistance, which is important to the bolometric mechanism. It considered several potential applications, including high-bit-rate quantum communication and cryptography, quantum LIDAR, and dark matter axion detection. A device has been fabricated to the extent of sandwiching magic-angle twist graphene between hBN gate dielectrics atop a back gate. Millimeter-wave antennas have been fabricated with a thermocouple junction at the feed for measurement of antenna function. A plan for cryogenic testing down to 40 mK has been formulated, and access to all necessary experimental apparatus has been secured. A tunable backward wave oscillator (160 GHz to 1.4 THz) has been acquired for characterization, and its functionality for determining resonant response of selective antenna coupled detectors demonstrated.

References

1. G. H. Lee, D. K. Efetov, W. Jung, L. Ranzani, E. D. Walsh, T. A. Ohki, T. Taniguchi, K., Watanabe, P. Kim, D. Englun, and K. C. Fong, “Graphene-based Josephson junction microwave bolometer,” Nature 586, 42 (2020), https://doi.org/10.1038/s41586-020-2752-4.
2. R. Kokkoniemi J.-P. Girard, D. Hazra, A. Laitinen, J. Govenius, R. E. Lake, I. Sallinen, V. Vesterinen, M. Partanen, J. Y. Tan, K. W. Chan, K. Y. Tan, P. Hakonen, and M. Möttönen, “Bolometer operating at the threshold for circuit quantum electrodynamics,” Nature 586, 47 (2020), https://doi.org/10.1038/s41586-020-2753-3.

3. E. D. Walsh, W. Jung, G.-H. Lee, D. K. Efetov, B.-I. Wu, K.-F. Huang, T. A. Ohki, T. Taniguchi, K. Watanabe, P. Kim, D. Englund, K. C. Fong, "Josephson junction infrared single-photon detector," Science. 372, 409 (2021), DOI: 10.1126/science.abf5539.
4. E. D. Walsh, D. K. Efetov, G.-H. Lee, M. Heuck, J. Crossno, T. A. Ohki, P. Kim, D. Englund, and K. C. Fong, "Graphene-Based Josephson-Junction Single-Photon Detector," Phys. Rev. Appl. 8, 024022 (2017), DOI: 10.1103/PhysRevApplied.8.024022.
5. X. Du, D. E. Prober, H. Vora, and C. B. Mckitterick, "Graphene-based Bolometers Graphene," 2D Mater. 1, 1 (2014), DOI 10.2478/gpe-2014-0001.
6. G. Di Battista, P. Seifert, K. Watanabe, T. Taniguchi, K. C. Fong, A. Principi, and D. K. Efetov, "Revealing the Thermal Properties of Superconducting Magic-Angle Twisted Bilayer Graphene," Nano Lett. 22, 6465−6470 (2022) https://doi.org/10.1021/acs.nanolett.1c04512
7. J. M. Park, Y. Cao, L. Q. Xia, L-Q, Xia, S. Sun, K. Watanabe, T. Taniguchi, and P. Jarillo-Herrero, "Robust superconductivity in magic-angle multilayer graphene family," Nat. Mater. 21, 877 (2022), https://doi.org/10.1038/s41563-022-01287-1
8. P.L. Richards, "The Josephson Junction as a Detector of Microwave and Far-Infrared Radiation," Chapter 6 in Semiconductors and Semimetals Volume 12, edited by R.K. Willardson and Albert C. Beer (Elsevier, 1977), Pages 395-440.
9. F. J. Gonzalez, M. S. Lodge, M. Ishigami, R. A. Klemm, A. Rathod, K. L. Lina, A. C. Bowman, F. Hernandez, C. J. Fredricksen, C. Cariker, R. E. Peale, "Antenna-coupled graphene josephson-junction terahertz detector," MRS Advances, published online 22 March 2023.
10. C. Hagmann, P. Sikivie, N. S. Sullivan, D, B. Tanner, "Results from a search for cosmic axions," Phys. Rev. D 42 1297 (1990).
11. ADMX web page http://www.phys.washington.edu/groups/admx/home.html
12. C. H. Bennett, G. Brassard, "Quantum cryptography: Public key distribution and coin tossing," Theor. Comp. Sci. 560, 7 (2014), http://dx.doi.org/10.1016/j.tcs.2014.05.025.
13. V. F. Guedes, F. A. Mendonca, J. B. R. Silva, R. V. Ramos, "Discrete variable quantum key distribution in millimeter-wave and THz regions," TechRxiv. Preprint. (2021), https://doi.org/10.36227/techrxiv.15091338.v1
14. F. J. González, G. D. Boreman, "Comparison of Dipole, Bowtie, Spiral and Log-periodic IR Antennas," Infrared Phys. & Technol. 46, 418 (2005), https://doi.org/10.1016/j.infrared.2004.09.002.
15. C. A. Balanis, Antenna Theory: Analysis and Design, 3rd ed. (Wiley, Hoboken, NJ, 2005).
16. D. Luong, B. Balaji, C. Wai, S. Chang, V. Manjunath, A. Rao and C. Wilson, "Microwave Quantum Radar: an Experimental Validation," IEEE Proc. 2018 International Carnahan Conference on Security Technology (ICCST), 22-25 October 2018, Montreal, QC, Canada DOI: 10.1109/CCST.2018.8585630.
17. S. Calhoun, R. Evans, I. O. Oladeji, J. Cleary, E. M. Smith, R. E. Peale, "Vanadium Oxide Thin Film by Aqueous Spray Deposition," MRS Advances 3, 2777 (2018).
18. A. C. Gadelha, D. A. A. Ohlberg, F. C. Santana, G. S. N. Eliel, J. S. Lemos, V. Ornelas, D. Miranda, R. B. Nadas, K. Watanabe, T. Taniguchi, C. Rabelo, P. Paulo de Mello Venezuela, G. Medeiros-Ribeiro, A. Jorio, L. G. Cançado, and L. C. Campos, "Twisted Bilayer Graphene: A Versatile Fabrication Method and the Detection of Variable

Nanometric Strain Caused by Twist-Angle Disorder," ACS Appl. Nano Mater. 4, 1858 (2021), https://doi.org/10.1021/acsanm.0c03230

19. Garcia, A. G. F., Neumann, M., Amet, F., Williams, J. R., Watanabe, K., Taniguchi, T., and Goldhaber-Gordon, D., "Effective Cleaning of Hexagonal Boron Nitride for Graphene Devices," Nano Letters 12, 4449 (2012).
20. L. Wang, I. Meric, P. Y. Huang, Q. Gao, Y. Gao, H. Tran, T. Taniguchi, K. Watanabe, L. M. Campos, D. A. Muller, J. Guo, P. Kim, J. Hone, K. L. Shepard, C. R. Dean, "One-Dimensional Electrical Contact to a Two-Dimensional Material," Science 342, 614 (2013).
21. H. Hashiba, V. Antonov, L. Kulik, A. Tzalenchuk, S. Komiyama, "Sensing individual terahertz photons," Nanotechnology 23, 165203 (2010), doi:10.1088/0957-4484/21/16/165203.
22. Chris Arose, "Spectrally selective pyroelectric detectors for THz sensing," PhD Dissertation (UCF, 2023).